Optical and Quantum Electronics (2020) 52:294
https://doi.org/10.1007/s11082-020-02391-9

Numerical estimation of lattice strain, bending and generation of misfit dislocations in CdHgTe heterostructures grown on GaAs substrate

Alina Jóźwikowska[1] · Olga Markowska[2] · Krzysztof Jóźwikowski[2]

Received: 6 August 2019 / Accepted: 5 May 2020 / Published online: 27 May 2020
© The Author(s) 2020

Abstract
Using our own computer program, we determined the spatial distribution of lattice strains in the HgCdTe heterostructure grown on a GaAs substrate. Lattice stress resulting from lattice mismatch between the substrate and the epitaxial layer and bending of the heterostructure is almost completely relaxed by misfit dislocations forming matrixes in the interfaces' areas. The average distances between dislocation lines in individual interfaces were calculated based on the minimum energy, i.e. elastic energy condition resulting from the interaction of stress fields and deformations caused by lattice misfit, bending and the presence of dislocation plus electrical energy of dislocations.

Keywords CdHgTe heterostructures · Lattice strain · Bending · Misfit dislocations

1 Introduction

Earlier, the basic research was focused on the growth, doping and characterization of MCT on lattice matched CdZnTe substrates because the highest crystal perfection is realized just for this material conjugation. But the crystal perfection and Zn content are not uniform over the surface area. Also, CdZnTe substrates are expensive and is issue with precise impurity control at growth. The alternative substrates (epilayers of CdTe on GaAs or Si substrate) have the advantages in comparison with CdZnTe substrates from the point of view of substrate dimension and low cost. The only problem is the mismatch between

This article is part of the Topical Collection on Numerical Simulation of Optoelectronic Devices.

Guest edited by Angela Thränhardt, Karin Hinzer, Weida Hu, Stefan Schulz, Slawomir Sujecki and Yuhrenn Wu.

✉ Krzysztof Jóźwikowski
krzysztof.jozwikowski@wat.edu.pl

[1] Faculty of Applied Informatics and Mathematics, Warsaw University of Life Science SGGW, Nowoursynowska 166 St., 02-787 Warsaw, Poland

[2] Faculty of Advanced Technologies and Chemistry, Military University of Technology, gen. S. Kaliskiego 2 St., 00-908 Warsaw, Poland

GaAs and the epitaxial layer. The resulting lattice stress can be effectively reduced by mismatch dislocations. The use of a buffer layer with CdTe allows them to be isolated from the epitaxial CdHgTe layer. As substrates for epitaxial CdHgTe layers, GaAs with crystallographic orientation (100) or (111) is often used (Ponce et al.1986). Other crystallographic orientations are also used. For example, (Sidorov et al. 2015) had grown epitaxial layers of MCT on GaAs (013) and Si (013) substrates and introduced the ZnTe and CdTe buffer layers which made it possible to retain the orientation close to that of the substrate in MCT despite of the large mismatch between the lattice parameters. By using the transmission electron microscopy, they found the network of misfit dislocations in substrate-buffer interface and measured the angles of rotation of the lattice due to the formation of networks of misfit dislocations. It is probably one of the causes of generation of threading dislocations in the epitaxial layer. Undoubtedly, this mechanism is a real challenge for developing a method of determining the density of treading dislocations from the condition of minimum elastic energy. In this papier we managed to propose such a method for the case of misfit dislocation. In the joint laboratory of Military University of Technology (MUT) and Vigo-System (V-S), the CdHgTe heterostructures are growing by using the Metal Organic Chemical Vapor Deposition (MOCVD) method (Kopytko et al. 2016). CdTe is used as the buffer layer. Strong lattice misfit between GaAs and CdTe is the cause of lattice stress causing the deformation of the crystal lattice of both the substrate and CdTe. Significant relaxation of stress occurs due to the misfit dislocations arising in the interfaces. Dislocations are generated in the form of a network with the same spacing between the dislocation lines lying in the planes of growth. If on CdTe we embed the $Cd_{1-x}Hg_xTe$ hererostructure, although the lattice misfit of the individual hetero-structural layers is relatively small, misfit dislocations also occur in areas where there is a change in molar composition x (Yamamoto et al.1985; Nouruzi-Khorasani et al. 1989). These dislocations and treading dislocations introduce additional energy states in the energy gap, and they create an additional channel for the generation and recombination processes described by the Shockley-Hall-Read (SHR) mechanism (Yamamoto et al. 1985, Pelliciari and Baret 1987; Virt et al. 2001; Gopal and Gupta 2003; Jóźwikowski et al. 2012). Thus, if we perform numerical simulations of infrared detectors built from these heterostructures, we should evaluate the density of these dislocations to properly calculate the generation and recombination rates of electric carriers. The rate of SHR processes is influenced by the polarization of the detectors, mainly through the trap assisted tunneling (TAT) mechanism. This effect is perfectly visible on the current–voltage characteristics of the devices being manufactured, and they confirm that in many cases the dislocation density determines photoelectric parameters of infrared detectors (Jóźwikowski et al. 2010). I our previous work (Jóźwikowska et al. 2019) we presented how to calculate pseudomorphic lattice strains in InAsSb heterostructures and deformations caused by bending the structure. In addition, we determined how thickness of the substrate and buffer affects the amount of lattice strain and density of the generated dislocations. We are not aware of any other works in which the density of misfit dislocations in all interfaces of a multi-layer heterostructure was theoretically determined. We verified the results of our calculations with the experimental data of (Kim and Raseghi 1998) and (Xie et al. 2018). In this work, we used the same methods for a CdHgTe heterostructure. The generated mismatch dislocations have both elastic energy and electrical energy. However, in our previous article we did not analyze the impact of electrical energy. We did it in this work. Our motivation for this work was to provide a theoretical explanation why in HgCdTe heterostructures embedded on GaAs substrates deformations are minimal, despite a large network mismatch. In addition, we wanted to determine the effect of electrical energy of misfit dislocations on their density.

2 Results and simulation procedure

Now we analyze CdHgTe heterostructures in the form of an epitaxial layers deposited on (100) GaAs substrate. The modeled structure has a shape of a cylinder of a diameter of 300 µm. Material parameters are presented in Fig. 1. The structures in this configuration are grown in joint laboratory of MUT-V-S and used for the construction of infrared detectors. In real structures there are no abrupt changes in parameters due to the diffusion of the elements forming CdTe and $Cd_xHg_{1-x}Te$ with different molar compositions x. The GaAs-CdTe interface is abrupt. This interface has the highest mismatch dislocation density. We can theoretically calculate it and determine the size of the lattice deformations relaxed by these dislocations. This is important when designing infrared detectors, because dislocations can significantly affect the lifetime of carriers and deformations change the position of the valence and conductivity band edges. Using our own computer program, we calculated lattice strains, and determined if there are pseudomorphic strains which give the same value of the lattice constant $a_{\parallel}$ in the plane of layers growth in all structure. Then we calculate the bending to determine the additional change in the lattice constant caused by this effect. Emerging deformations of the crystalline lattice cause stresses that are greatly relaxed by the misfit dislocations arising in the interfaces.

If the epitaxial layer contains dislocations with the average inter-dislocation distance p, the expression for strain becomes (Jóźwikowska et al. 2019).

$$\epsilon_{\parallel}(z) = \frac{a_{\parallel} - a(z)}{a(z)} + \frac{z - h_b}{R} - \sum_{i=1}^{n} \delta(h_i) b_1(h_i)/p(h_i) \tag{1}$$

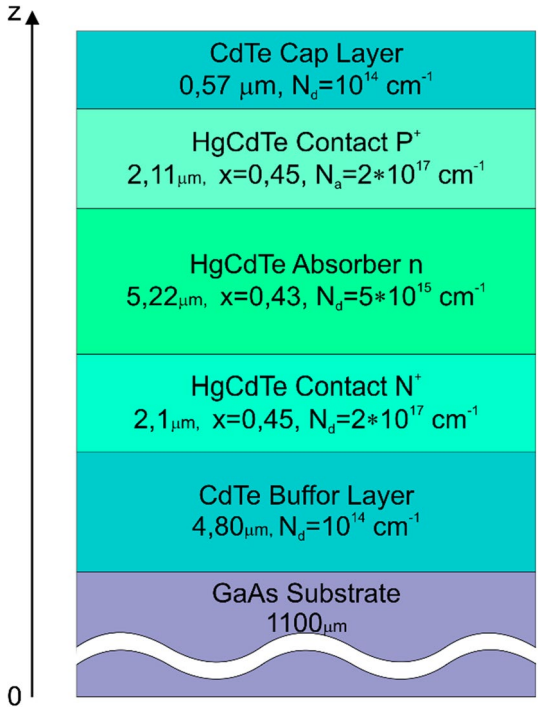

Fig. 1 HgCdTe photodetector P^+nN^+ structure grown on (001) GaAs substrate using the MOCVD method

The first component describes the strain caused by the pseudomorphic lattice constant ($a_{\parallel}$), parallel to the plain of interface, which remains the same throughout the structure and $a(z)$ denotes the unstrained lattice constant. The second component specifies the deformation caused by bending. Only the bending enables achieving the balance of momenta of the internal forces due to the appearance of an additional stress, which partially changes the stress responsible for the formation of a pseudomorphic structure. Some of the layers are subject to an additional tensile and some to an additional compression. There is precisely one layer that will retain its size. h_b is it's distant from the bottom of the structure. The bottom of the heterostructure has curvature of radius R. In (Jóźwikowska et al. 2019) we have obtained the expressions:

$$a_{\parallel} = \frac{\int_0^h \frac{G(z)}{a(z)} dz}{\int_0^h \frac{G(z)}{a^2(z)} dz}; \quad R \approx \frac{\int_0^h zG(z) \frac{a_{\parallel}}{a(z)} dz}{\int_0^h G(z)\left(1 - \frac{a_{\parallel}}{a(z)}\right) dz}; \quad h_b = \frac{\int_0^h G(z)(R+z)^2 \frac{a_{\parallel}}{a(z)} dz}{\int_0^h G(z)(R+z) dz} - R \tag{2}$$

where h is the thickness of the structure and G is the Young's modulus.

Misfit dislocations generated in interface areas significantly reduce crystal lattice deformation (third component in formula (1). In this term $b_1 = -b \sin\alpha \sin\beta$ and b is norm of the Burger's vector, h_i is the z coordinate of the i-th interface, $p(h_i)$ denotes the mean distance between misfit dislocation lines in the i-th interface.

For 60° dislocations

$$\alpha = \arctan \frac{1}{\sqrt{2}}, \quad \beta = \frac{\pi}{3} \tag{3}$$

δ takes values 1 or -1, so that $\epsilon_{\parallel}$ takes usually lower values than the values specified by the first two components in the expression (1).

All these quantities in Eq. 1 were derived in our earlier paper (Jóźwikowska et al. 2019).

The elastic energy per unit area of the heterostructure is expressed by the dependence (after Gosling et al. 1993; Jain et al. 1993, 1997; Jóźwikowska et al. 2019)

$$\begin{aligned} E_{elst} = {} & \frac{1}{2} \int_0^h B(z) \left(\frac{a_{\parallel} - a(z)}{a(z)} \right)^2 dz + \frac{1}{2} \sum_{i=1}^{5} \left(\frac{b_1(h_i)}{p(h_i)} \right)^2 \int_{h_i}^{h} B(z) dz \\ & + \sum_{i=1}^{5} \frac{b_1(h_i)}{p(h_i)} \int_{h_i}^{h} B(z) \left(\frac{a_{\parallel} - a(z)}{a(z)} \right) dz \\ & + \sum_{i=1}^{4} \frac{b_1(h_i)}{p(h_i)} \left(\sum_{j=i+1}^{5} \frac{b_1(h_j)}{p(h_j)} \int_{h_j}^{h} B(z) dz \right) \end{aligned} \tag{4}$$

And electrical energy of misfit dislocations deposited in five interfaces of the heterostructure shown in Fig. 1 per unit area reads

$$E_{elctr} = 2\pi\varepsilon_0 \sum_{i=1}^{5} \frac{1}{p_i} \int_0^{r_{i_m}} \varepsilon(r) \left(\frac{\partial \Psi_i}{\partial r} \right)^2 r dr \tag{5}$$

where Ψ is the electrical potential, ε_0 is the vacuum permittivity, and $\varepsilon(r)$ is the relative dielectric permittivity. Counting the minimum energy $E_{elst} + E_{elctr}$ as a function of $p(h_i)$, we numerically determine the values of $p(h_1)$, $p(h_2)$ $p(h_3)$,$p(h_4)$ and $p(h_5)$ and then using the expression (1) we obtain strain $\epsilon_{\|}(z)$ as a function of thickness. Earlier we performed similar calculations for heterostructures with InAsSb deposited on a GaAs and GaAs substrate in two papers (Jóźwikowska et al. 2019, Jóźwikowska, Suligowski. 2019). In the above works, we have described in detail the method used for calculating the edges of energy bands and the distances between misfit dislocation lines in the interfaces. In this paper, additionally we estimated the energy of the electric field generated around misfit dislocations. To do this we determined the spatial distribution of electrical potential by solving the Poisson equation in cylindrical regions around dislocations' cores. However, this additional energy is small compared to the elastic energy and practically has no significant effect on the density of generated misfit dislocations. We have also determined the statistical distribution function for the electrons in the dislocation bands formed by dislocation electron states. Determination of the distribution function is very important if we want to consider the effect of the misfit dislocation on the carrier lifetime (Jóźwikowski et al. 2010).

Figure 2 shows the spatial distribution of the lattice strain in the GaAs substrate. Pseudomorphic strains are constant and take values $\varepsilon_{\|}$ slightly above 0.05%. These are stretching strains. The bending of the structure, necessary to achieve the condition of the equilibrium of moments of internal forces, causes the deformation character in the bottom layer of the substrate to change, squeezing it, while the top layer is stretched (red line in Fig. 2). At a distance of $h_b = 550.4$ µm from the bottom, there is the layer not deformed by bending.

The bending radius is 18.55 cm. Pseudomorphic strains in the epitaxial layer are compressive and amount to over 12%. The bending of the epitaxial structure slightly reduces strains by a fraction of a percent (blue line in Fig. 3).

The generated misfit dislocations have a very strong effect on the relaxation of the lattice stress and reduction of deformations in the individual layers of the heterostructure

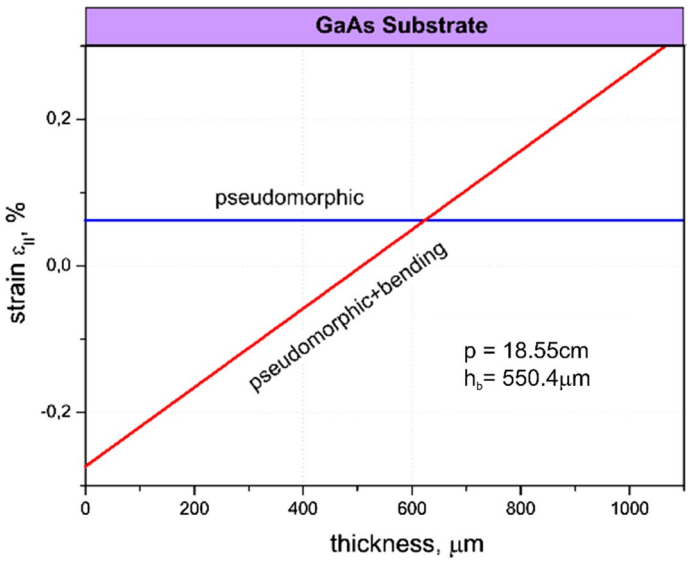

Fig. 2 Distribution of strains $\varepsilon_{\|}$ at the GaAs substrate with a thickness of 1100 µm. Blue line refers to the pseudomorphic strains. Red line refers strains with additional bending of the structure

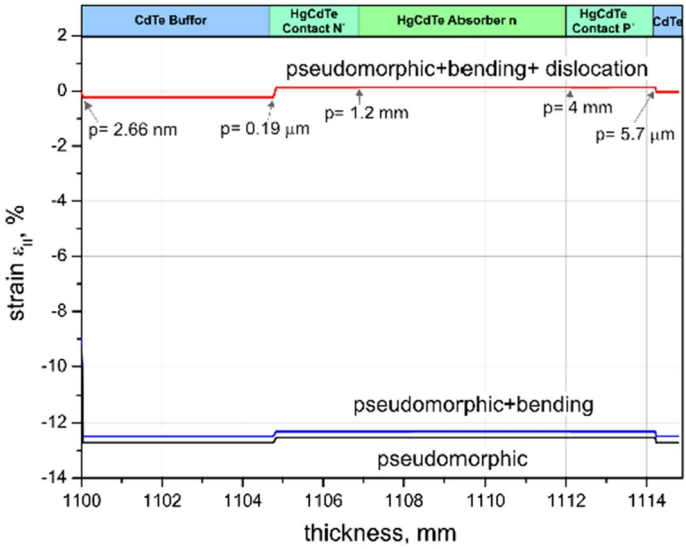

Fig. 3 Spatial distribution of strains $\varepsilon_{\parallel}$ at the HgCdTe epitaxial layer at 300 K deposited on GaAs (100) substrate

(Fig. 3). Figure 3 also shows the parameter p, which is the average distance between misfit dislocation lines in the interface areas between the epitaxial layers. A very dense grid of dislocations (p = 2.66 nm) is at the border buffer-substrate. However Ponce et al. studied the interface structure of CdTe(100)/GaAs(100) obtained by growing thin CdTe films on GaAs (100) by molecular beam epitaxy. By using high-resolution transmission electron microscopy, they found the presence of two-dimensional dislocation network at the

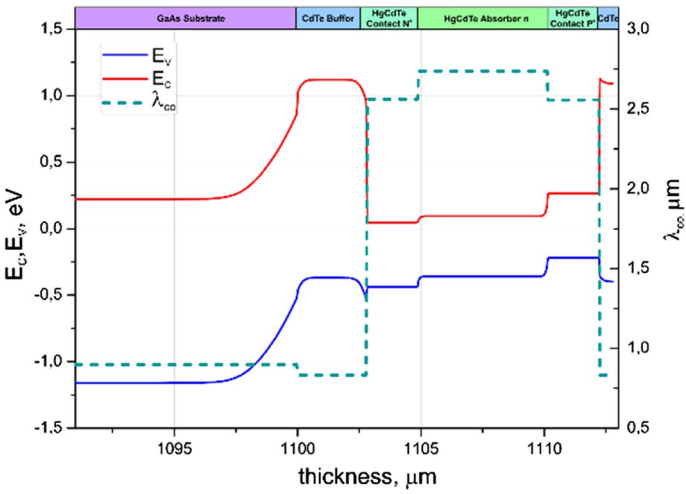

Fig. 4 Calculated band structure as a function of thickness in the epitaxial layer (solid lines). Dashed line shows spatial distribution of cut off wavelength λ_{co}

interface. The dislocations run along ⟨110⟩ directions in the interface with periodicity of 3.1 nm. The result of our calculations ($p = 2.66$ nm) is very similar to their experimental result. Fortunately, in the other interfaces of the heterostructure analyzed by us, the density of dislocations is by orders of magnitude smaller. Figure 4 shows the spatial distribution of the edges of energy bands and the cut off wavelength $\lambda_{co} = 1.24/E_g$ in the substrate and epitaxial layers, taking into consideration the influence of lattice deformations on the position of the band edges. The calculated distribution of electric charge of dislocation cores (see "Appendix") enables to estimate the electric charge density of the order of $5x10^{12}$ cm^2 in the GaAs-CdTe interface. However, the dislocation cores are substantially shielded by the free carriers and the ionized dopants which results in a significant reduction of the resultant electric charge in the interface area. Figure 4 does not include the impact of this charge on the potential distribution. It is expected that the overall charge is small enough that it will not significantly influence the shape of the obtained sheet. Even if we include it in our considerations, it will change the distribution of the band edges only in the GaAs-CdTe interface area and will not affect the course of the band structure in the other more important layers of the heterostructure.

Figure 5 presents the intensity of the electric field E as a function of the distance from the line of a dislocation α. The calculations were made for dislocations which could exist in the GaAs substrate and in all deposited layers shown in Fig. 1. The method of calculating the electric field strength around the dislocation core is presented in the "Appendix". Knowing it, we can calculate the electrical energy per unit area (see Eq. (7) in "Appendix"). We assumed that the average electron energy in the dislocation bands in CdHgTe layers and CdTe buffer are above the apex of the valence band at a distance $E_{DIS} = 0.32E_g$.). After (Wosinski and Figielski 1993) we assumed that E_{DIS} in GaAs substrate is lying 0.68 eV below the conduction band.

The calculated electrical energies of dislocation per unit area fall within the range $10^{-7} \div 10^{-5}$ J cm^{-2}. These values are many orders of magnitude smaller than the elastic energy expressed by the relation (4). (Ciura et al.2016) had investigated the trap levels

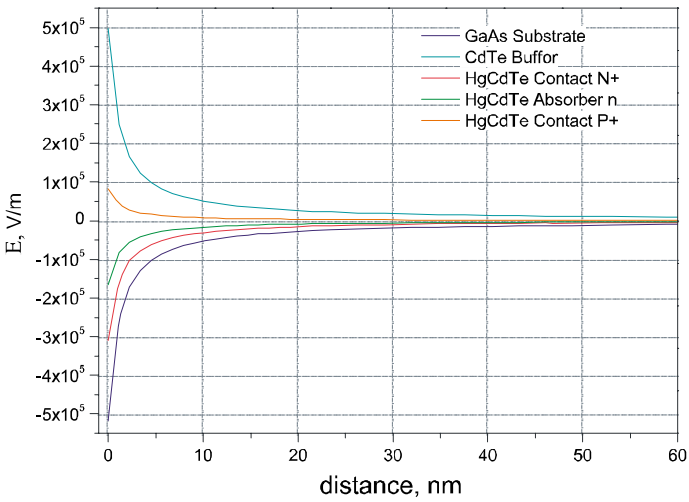

Fig. 5 The electric field intensity as a function of the distance from the dislocation lines, lying in particular layers of the heterostructure shown in Fig. 1

in HgCdTe heterostructures which were MOCVD grown on (111) CdTe buffered (100) GaAs substrates at VIGO S.A. laboratories with low frequency noise spectroscopy. Apart from the hole traps, three electron traps were also found. Their energy levels follow the trend lines $E_T = 0.75Eg$ and $E_T = 0.35Eg$. The first line is easy to identify as the line associated with mercury vacancies. The second line was not identified by the authors and is probably associated with dislocations. This trend line is very close to the value assumed by us $E_{DIS} = 0.32E_g$. Using this value, we calculated the carrier lifetime and obtained a good fit to the experimental current–voltage characteristics of HgCdTe photodiodes in many of our previous works, e.g. (Jóźwikowski et al. 2010).

Physical parameters of GaAs used in the calculations were taken from work (Vurgaftman et al. 2001), and of CdTe and HgCdTe from monographs (Capper 1994 and Capper and Garland 2011).

3 Conclusions

Including misfit dislocations in the calculations of strains allows to estimate the real mechanisms of the lattice relaxation. By computing the minimum energy, we can numerically determine the values of average distances between misfit dislocations lines in the interfaces of HgCdTe heterostructures. The calculation methods used here are described in detail in our two earlier works. In this work as a novelty we presented the numerical method of calculating the spatial distribution of electrostatic potential around the dislocation core and calculating the statistical distribution function of electrons in the dislocation band. We also estimated the amount of electrical energy in the area surrounding the core of dislocations α and β in CdHgTe. We added it to the total elastic energy connected with the lattice stress. Its share, however, is insignificant and does not affect the density of misfit dislocations in interfaces of considered hererostructure.

Acknowledgements The work has been done under financial support of the Polish National Science Centre as research Projects No. 2016/23/B/ST7/03958 and 2016/23/N/ST7/03618.

Open Access This article is licensed under a Creative Commons Attribution 4.0 International License, which permits use, sharing, adaptation, distribution and reproduction in any medium or format, as long as you give appropriate credit to the original author(s) and the source, provide a link to the Creative Commons licence, and indicate if changes were made. The images or other third party material in this article are included in the article's Creative Commons licence, unless indicated otherwise in a credit line to the material. If material is not included in the article's Creative Commons licence and your intended use is not permitted by statutory regulation or exceeds the permitted use, you will need to obtain permission directly from the copyright holder. To view a copy of this licence, visit http://creativecommons.org/licenses/by/4.0/.

Appendix

Electrical energy of dislocations

Figure 6 shows a diagram of the dislocation band formed by energy states associated with unsaturated bonds of the dislocation core. We assumed that the distance between these bonds is equal to b, the length of the Burger's vector, which for dislocation line of length equal to l gives, due to spin degeneration, the number of states in the band equal to $2\frac{l}{b}$. When the dislocation core is electrically neutral, some of these energy levels are filled with

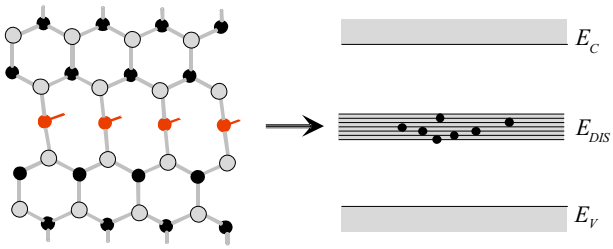

Fig. 6 A model of dislocation band formed by unsaturated bonds of atoms in the dislocation core

electrons in the amount resulting from the semiconductor type and equal to $\xi \frac{l}{b}$. And so, for atoms from the fourth group $\xi = \frac{1}{2}$, for dislocation α in $A_{II}B_{VI}$ compounds we should get $\xi = \frac{4}{6}$, and for dislocation β $\xi = \frac{2}{6}$, respectively. Similarly, for $A_{III}B_V$ compounds $\xi = \frac{5}{8}$ for α and $\xi = \frac{3}{8}$ for β. Due to the role of ionic bond in semiconductor compounds, the ξ parameter may differ slightly from those given herein. For example, assuming the same ionicity of bonds for all $A_{III}B_V$ compounds, (Masut et al. 1982)] received $\xi_\alpha \cong 0.83$ and $\xi_\beta \cong 0.17$. It is possible to pass electrons from the areas surrounding the dislocation line to the dislocation band as well as from the dislocation band to the surrounding area. Then, instead of the parameter ξ, we will use the parameter n_{DIS} specifying the number of electrons in the dislocation band. We assumed that the average energy value of the dislocation band is E_{DIS} above the apex of the valence band (Jóźwikowski et al. 2012).

The energy accumulated in the electrical field formed by a dislocation core with the length l reads

$$E_{el} = \frac{1}{2}\varepsilon_0 l \int_0^{r_m} \left(\frac{\partial \Psi}{\partial r}\right)^2 \varepsilon_r 2\pi r dr \tag{6}$$

The AB and CD segments contribute to the electrical energy of dislocations lying in a rectangular plane element marked with a dotted line. $l = 2p$. Thus, the amount of electrical energy per unit area reads (Figs. 7, 8)

$$\check{E}_{el} = \frac{2\pi}{p}\varepsilon_0 \int_0^{r_m} \varepsilon(r)\left(\frac{\partial \Psi}{\partial r}\right)^2 r dr \tag{7}$$

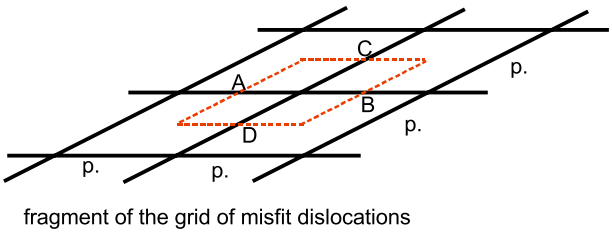

Fig. 7 The electrical potential around the dislocation line is counted in a cylinder with a radius r_m equal to half the distance between the dislocation lines

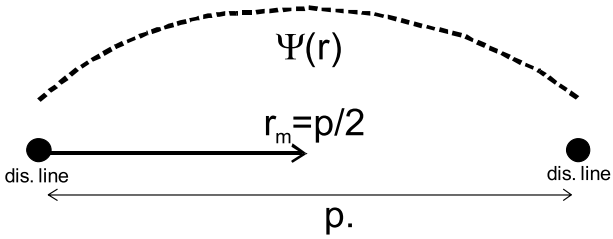

Fig. 8 A fragment of the grid created by misfit dislocations

Calculation of the electrostatic potential

The free Helmholtz energy $F = E - TS$ of the dislocation core per the unit of length reads

$$F = \left(\frac{n_{DIS}}{l} - \xi\frac{1}{b}\right)\left(E_V(0) - e\Psi(0) + E_{DIS} - \Phi\right) + \frac{1}{2}\varepsilon_0\varepsilon_r\int_0^{r_m}\left(\frac{\partial\Psi}{\partial r}\right)^2 2\pi r dr - k_B T\left[\left(2\frac{1}{b}\right)! - \left(\frac{n_{DIS}}{l}\right)!\left(2\frac{1}{b} - \frac{n_{DIS}}{l}\right)!\right] \tag{8}$$

The first two components in the Eq. (8) refer to the energy of electrons, and the third is their entropy S multiplied by temperature T. n_{DIS} is the number of occupied electron states in dislocation with length l.

From condition, that $\frac{\partial F}{\partial\left(\frac{n_{DIS}}{l}\right)} = 0$ and using the Strirling's relation $\ln(n!) = n \cdot \ln(n) - n$, one obtains the relation

$$\frac{n_{DIS}}{l} = \frac{2}{b}\Big/\left[1 + exp\left(\frac{E_V(0) - e\Psi(0) + E_{DIS} - \Phi}{k_B T}\right)\right] \tag{9}$$

where E_V is the edge of the valence band, Φ is the Fermi energy, and b is the Burger vector assumed to be equal the lattice constant a.

To obtain $\frac{n_{DIS}}{l}$ we need to calculate the value of electrical potential $\Psi(0)$, in the dislocation core. To do this, we must solve the Poisson equation in the area surrounding the dislocation core and consider the electrical charge that is there. The Poisson equation is solved iteratively by the Newton's method:

$$\Psi_{n+1}(r) = \Psi_n(r) + \delta\Psi_n(r) \tag{10}$$

Where $\Psi_{n+1}(r)$ is the potential value after the n-th iteration, and $\delta\Psi_n(r)$ is the n-th iterative correction. It is crucial to determine the initial potential values. We determine these from the local condition of electrical neutrality at every point of the structure. It also depends on the value of Fermi energy. Under conditions of thermal equilibrium, the value $\Phi = 0$ should be used.

Electrical neutrality in the dislocation core will occur when:

$$\frac{n_{DIS}}{l} = \xi\frac{1}{b} = 2\frac{1}{b}\Big/\left[1 + exp\left(\frac{E_V(0) - e\Psi(0) + E_{DIS} - \Phi}{k_B T}\right)\right] \tag{11}$$

From here we get initial value of potential in dislocation core

$$e\Psi_1(0) = E_V(0) + E_{DIS} - \Phi - ln\left(\frac{2-\xi}{b}\right)k_B T \tag{12}$$

However, in the area surrounding the dislocation line, the initial potential is determined numerically from the condition:

$$\rho(r) = p\left(\Psi_1(r)\right) - n\left(\Psi_1(r)\right) + N_D^+\left(\Psi_1(r)\right) - N_A^-\left(\Psi_1(r)\right) = 0 \tag{13}$$

Where concentration of electrons, holes, ionized donors and ionized acceptors is expressed as below:

$$p\left(\Psi_1(r)\right) = \frac{1}{4\pi^3}\int_{BZ} 1/\left[1 + exp\left(\frac{\Phi - E_V(r) + e\Psi_1(r) + \varepsilon_V^k\left(\vec{k}\right)}{k_B T}\right)\right]d^3k \tag{14}$$

$$n\left(\Psi_1(r)\right) = \frac{1}{4\pi^3}\int_{BZ} 1/\left[1 + exp\left(\frac{E_V(r) + E_g(r) - e\Psi_1(r) + \varepsilon_C^k\left(\vec{k}\right) - \Phi}{k_B T}\right)\right]d^3k \tag{15}$$

$$N_A^-\left(\Psi_1(r)\right) = N_A/\left[1 + \frac{g_{0A}}{g_{1A}}exp\left(\frac{E_V(r) - e\Psi_1(r) + E_A(r) - \Phi}{k_B T}\right)\right] \tag{16}$$

$$N_D^+\left(\Psi_1(r)\right) = N_D/\left[1 + \frac{g_{1D}}{g_{0D}}exp\left(\frac{\Phi - E_V(r) - E_g(r) + e\Psi_1(r) + E_D(r)}{k_B T}\right)\right] \tag{17}$$

k is the wave vector, ε_V^k and ε_V^k is the kinetic energy of holes and electrons respectively, E_g is the width of the energy gap, T denotes temperature, k_B is the Boltzmann's constant, E_D and E_A is the ionization energy of donors and acceptors, respectively. BZ means integration in the first Brillouine's zone, N_A and N_D is the concentration of the acceptors and donors, respectively.

To find coefficients g_1 and g_0, you should know the type of orbitals present in the analyzed doping state. A thorough analysis of the degeneration of dopant states was made by D. Look in his book (Look 1989).

The potential was calculated numerically by solving the Poisson equation expressed by an equivalent diffusion equation (as in Jóźwikowska 2008):

$$\int_V \frac{\partial\Psi}{\partial t}dV = \varepsilon_0\oint \varepsilon_r\nabla\Psi dA + e\int_V \rho dV \tag{18}$$

where V denotes the volume of the ring of the ABCD cross-section, A is the ring's surface, ρ is the density of electric charge, ∇ is the gradient, and t is the pseudo time.

Due to the small volume of the ring we may, instead of integration, multiply $\frac{\partial\Psi}{\partial t}$ and ρ by the volume V of the ring. Similarly, $\varepsilon_r\nabla\Psi$ is multiplied by the surface of the ring.

Equation (17) in the cylinder of the radius around the core of dislocation takes the form

$$\frac{\partial \Psi(1)}{\partial t}\pi a^2 = \varepsilon_0 \varepsilon_r \nabla \Psi 2\pi a + e\left(\xi \frac{1}{b} - \frac{n_{DIS}}{l}\right) \tag{19}$$

But in the iterative equation we can write:

$$\frac{\partial \Psi(1)}{\partial t} = \frac{\Psi_{n+1}(1) - \Psi_n(1)}{\tau} = \frac{\delta \Psi_n(1)}{\tau} = L(\Psi_{n+1}) \cong \frac{1}{2}L(\Psi_{n+1}) + \frac{1}{2}L(\Psi_n) = L(\Psi_n) + \frac{1}{2}\frac{\partial L(\Psi_n)}{\partial \Psi_n}\delta \Psi_n \tag{20}$$

$$\text{where} \quad L(\Psi) = \frac{2\varepsilon_0 \varepsilon_r}{a}\nabla \Psi + \frac{e}{\pi a^2}\left(\xi \frac{1}{b} - \frac{n_{DIS}}{l_{DIS}}\right) \tag{21}$$

Thus, the Eq. (18) in the iterative form will be expressed as follows

$$\left\{\frac{1}{\tau} + \frac{\varepsilon_0 \varepsilon_r(1)}{2a^2} + \frac{e}{\pi a^2}\frac{\partial\left(\frac{n_{DIS}}{l}\right)}{\partial \Psi_n}\right\}\delta \Psi_n(1) - \frac{\varepsilon_0 \varepsilon_r(1)}{2a^2}\delta \Psi_n(2) = \frac{2\varepsilon_0 \varepsilon_r(1)}{a}\frac{\Psi_n(2) - \Psi_n(1)}{2a} + \frac{e}{\pi a^2}\left(\xi \frac{1}{b} - \frac{n_{DIS}}{l}\right) \tag{22}$$

which is the boundary condition at the point $r = 0$.

Potential Ψ was calculated in the central point S shown in Fig. 9. An example of cylindrical ring of a rectangular ABCD cross-section around a segment of the dislocation core of the length dz. For these rings, the difference scheme expressed by the Gauss theorem of calculus (as in Jóźwikowska 2008) was constructed to solve Eq. (17). The Neumann boundary condition for $r = r_m$

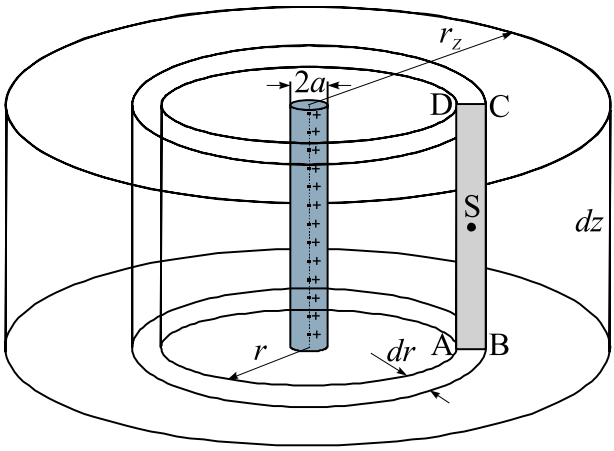

Fig. 9 We divide the area around the dislocation core into cylindrical rings with rectangular cross-sections. An example of such a ring with a rectangular section ABCD is shown in the picture. In these rings we solve the Poisson equation numerically. The area containing the core section of the dislocation core is a cylinder with a radius of a (lattice constant) containing an uncompensated electrical charge equal to $-e\left(n_{DIS} - \xi \frac{l}{b}\right)\frac{dz}{l}$

$$\left.\frac{\partial \Psi(0)}{\partial r}\right|_{r=r_m} = 0. \tag{23}$$

in the calculations we have achieved the convergence of the iterative method for $\tau = 10^{-4}$.

References

Capper, P. (ed.): Narrow Gap Cadmium-Based Compounds. INSPECT, IEE, London (1994)

Capper, P., Garlan, J. (eds.): Mercury Cadmium Telluride: Growth, Properties and Applications (Wiley Series in Materials for Electronic & Optoelectronic Applications). Wiley, New York (2011)

Ciura, L., Kolek, A., Kębłowski, A., Stanaszek, D., Piotrowski, A., Gawron, W., Piotrowski, J.: Investigation of trap levels in HgCdTe IR detectors through low frequency noise spectroscopy. Semicond. Sci. Technol. (2016). https://doi.org/10.1088/0268-1242/31/3/035004

Gopal, V., Gupta, S.: Effect of dislocations on minority carrier lifetime in HgCdTe. J. Appl. Phys. (2003). https://doi.org/10.1063/1.1644039

Gosling, T.J., Bullough, R., Jain, S.C., Willis, J.R.: Misfit dislocation distributions in capped (buried) strained semiconductor layers. J. Appl. Phys. (1993). https://doi.org/10.1063/1.353445

Jain, U., Jain, S.C., Nijs, J., Willis, J.R., Bullough, R., Mertens, R.P., Van Overstraeten, R.: Calculation of critical-layer-thickness and strain relaxation in Ge_xSi_{1-x} strained layers with interacting 60 and 90° dislocations. Solid State Electron. (1993). https://doi.org/10.1016/0038-1101(93)90084-4

Jain, S.C., Willander, M., Pinardi, K., Maes, H.E.: A review of recent work on stresses and strains in semiconductor heterostructures. Phys. Scr. (1997). https://doi.org/10.1088/0031-8949/1997/T69/009

Jóźwikowska, A.: Numerical solution of the nonlinear Poisson equation for semiconductor devices of a diffusion-equation finite difference scheme. J. Appl. Phys. (2008). https://doi.org/10.1063/1.2982275

Jóźwikowska, A., Jóźwikowski, K., Ciupa, R., Suligowski, M.: Estimation of influence of lattice strain, bending and doping on the width of energy gap in InAsSb heterostructures. Infrared Phys. Technol. (2019a). https://doi.org/10.1016/j.infrared.2019.04.020

Jóźwikowska, A., Suligowski, M., Jóźwikowski, K.: Enhanced numerical design of two-barrier infrared detectors with III–V compounds heterostructures considering the influence of lattice strain and misfit dislocations on the band gap. Optical and Quantum Electron **51**, 247 (2019b). https://doi.org/10.1007/s11082-019-1960-3

Jóźwikowski, K., Kopytko, M., Rogalski, A., Jóźwikowska, A.: Enhanced numerical analysis of current-voltage characteristics of long wavelength infrared n-on-p HgCdTe photodiodes. J. Appl. Phys. (2010). https://doi.org/10.1063/1.3483926

Jóźwikowski, K., Jóźwikowska, A., Kopytko, M., Rogalski, A., Jaroszewicz, L.R.: Simplified model of dislocations as a SRH recombination channel in the HgCdTe heterostructures. Infrared Phys. Technol. (2012). https://doi.org/10.1016/j.infrared.2011.10.003

Kim, J.D., Razeghi, M.: Investigation of InAsSb infrared photodetectors for near room temperature operation. Opto-Electron. Rev. **6**(3), 217–230 (1998)

Kopytko M., Jóźwikowski K., Martyniuk P., Gawron W., Madejczyk P., Kowalewski A., Markowska O., Rogalski A., Rutkowski.: J.:Status of HgCdTe barrier infrared detectors grown by MOCVD in Military University of Technology. J. Electron. Mater. (2016). https://doi.org/10.1007/s11664-016-4702-3

Look, D.C.: Electrical characterization of GaAs materials and devices. Wiley, New York (1989) (ch.1.4 and Apendix C)

Masut, R., Penchina, C.M., Farvacque, J.L.: Occupation statistics of dislocation deep levels in III-V compounds. J. Appl. Phys. **53**(7), 4964–4969 (1982). https://doi.org/10.1063/1.331332

Nouruzi-Khorasani, A., Jones, I.P., Dobson, P.S., Williams, D.J., Astles, M.G.: Transmission electron microscopy of LPE grown CdHgTe. J. Crystal Growth. (1989). https://doi.org/10.1016/0022-0248(89)90532-0

Pelliciari, B., Baret, G.: Role of dislocations in *n*-type annealed CdHgTe grown by liquid-phase epitaxy. J. Appl. Phys. (1987). https://doi.org/10.1063/1.339200

Ponce, F.A., Anderson, G.B., Balliangall, J.M.: Interface structure in heteroepitaxial CdTe on GaAs (100). Surf. Sci. (1986). https://doi.org/10.1016/0039-6028(86)90887-3

Sidorov, YuG, Yakushev, M.V., Varavin, V.S., Kolesnikov, A.V., Trukhanov, E.M., Sabinina, I.V., Loshkarev, I.D.: Density of Dislocations in CdHgTe Heteroepitaxial Structures on GaAs (013) and Si(013) Substrates. Phys. Solid State (2015). https://doi.org/10.1134/S1063783415110311

Virt, I., Bilyk, M., Khlyap, G., Shkumbatiuk, P., Kuzma, M., Dumanski, L.: Photoelectric properties of dislocations in $Hg_{1-x}Cd_xTe$ crystals. Proc. EDMO/Vienna (2001). https://doi.org/10.1109/EDMO.2001.974328

Vurgaftman, I., Mayer, J.R., Ram-Mohan, L.R.: Band parameters for III-V compound semiconductors and their alloys. J. Appl. Phys. (2001). https://doi.org/10.1063/1.1368156

Wosinski, T., Figielski, T.: Energy levels and electrical activity of dislocation electron states in GaAS. Acta Physica Polonica A (1993). https://doi.org/10.12693/APhysPolA.8351

Xie, C., Pusino, V., Khalid, A., Craig, A.P., Marshall, A., Cumming, D.R.S.: Monolithically integrated InAsSb-based nBnBn heterostructure on GaAs for infrared detection. IEEE J. Sel. Top. Quantum Electron. **24**, 1–6 (2018). https://doi.org/10.1109/JSTQE.2018.2828101

Yamamoto, T., Miyamoto, Y., Takinawa, K.: Minority carrier lifetime in region close to the interface between the anodic oxide and CdHgTe. J. Crystal Growth (1985). https://doi.org/10.1016/0022-0248(85)90156-3

Publisher's Note Springer Nature remains neutral with regard to jurisdictional claims in published maps and institutional affiliations.